Effect of temperature on polarization switching in long-wavelength VCSELs

Ana Quirce[a], Angel Valle*[b], Luis Pesquera[b], Krassimir Panajotov[a,c], Hugo Thienpont[a]
[a]Vrije Universiteit Brussel, Faculty of Engineering Sciences, Brussels Photonics Team B-PHOT, Pleinlaan 2, 1050, Brussels, Belgium;
[b]Instituto de Física de Cantabria, Consejo Superior de Investigaciones Científicas (CSIC)-Universidad de Cantabria, E-39005 Santander, Spain;
[c]Institute of Solid State Physics, 72 Tzarigradsko, Chaussee Blvd., 1784 Sofia, Bulgaria.

ABSTRACT

We have measured the effect of the temperature on the polarization-resolved characteristics of a 1550-nm single-transverse mode vertical-cavity surface-emitting laser (VCSEL). Two double polarization switchings (PS) are observed. For low temperatures a PS from longer to shorter wavelengths (Type II PS) followed by the opposite PS (Type I) is observed. For higher temperatures Type I followed by Type II PS are measured. A simple expression relating the spin flip rateto the dichroism, differential gain, threshold current and PS current is derived. With this expression the dependence of the spin-flip rate on the temperature is obtained.

Keywords: Vertical-cavity surface-emitting lasers (VCSELs), intrinsic parameters, polarization parameters, spin-flip model, dichroism, birefringence.

1. INTRODUCTION

Vertical-cavity surface-emitting lasers (VCSELs) are used in a large number of applications due to their important advantages over the edge-emitting lasers [1]. These include low threshold current, single longitudinal mode operation, compactness, low power consumption, and low cost [1,2]. Also their high power conversion efficiency and high modulation bandwidth allow VCSELs to be applied in high-volume data communication applications [3,4]. Long-wavelength VCSELs are gradually establishing themselves as key components for uncooled, low power, long-wavelength transceivers for decreasing the total power consumption in big data centers [4]. Although VCSELs are single-longitudinal mode devices, they usually show complex polarization characteristics [5-8] and multi-transverse mode dynamics [9,10]. The light emitted by the device is commonly linearly polarized along one of two orthogonal directions, and polarization switching (PS) between the two linearly polarized modes is often observed when changing the bias current or temperature. Most of the experimental works on PS in VCSELs have been performed on short-wavelength devices [1], [5], [7], [11-16]. Two types of PS, Type I PS (from the high to the low-frequency polarization) and Type II PS (from the low to the high-frequency polarization) have been found for 850-nm wavelength VCSELs [1], [7], [15]. Also double PS: Type I followed by Type II PS has been found in some short-wavelength devices [1], [7]. Less attention has been paid to polarization properties of long-wavelength VCSELs in which only Type I PS has been found [17-19].

In this work, we study the effect of the temperature on the polarization-resolved characteristics of a 1550 nm wavelength VCSEL. We find Type I and Type II PS in our device. We observe double polarization switchings, Type II followed by Type I PS and vice versa, depending on the temperature of the device. The Type II followed by Type I double PS is observed at low VCSEL temperatures and it has not been so far described in a VCSEL to the best of our knowledge. We characterize the VCSEL close to the PS region by measuring the non-linear dichroism, the nonlinear birefringence and the PS current as a function of the temperature. Also the differential gain and threshold current are obtained for different temperature values. We derive a simple expression that relates the previous quantities to the spin-flip rate of the device. In this way we obtain the temperature dependence of the VCSEL spin-flip rate, a very important parameter for determining the polarization properties of the device.

*valle@ifca.unican.es; phone 34 942 201465; fax: 34 942 200935

Vertical-Cavity Surface-Emitting Lasers XIX, edited by Chun Lei, Kent D. Choquette, Proc. of SPIE
Vol. 9381, 93810X · © 2015 SPIE · CCC code: 0277-786X/15/$18 · doi: 10.1117/12.2079742

The paper is organized as follows. In section II we describe the theoretical model and we derive an expression for the spin-flip rate. In section III we present the experimental results obtained for polarization-resolved characteristics . Section IV describes the polarization parameters of the VCSEL as a function of the temperature. Finally, in section V, a summary is presented.

2. THEORETICAL MODEL

The first part of our analysis considers the Spin Flip Model (SFM) [6], [20]. The model equations are given by [19]:

$$\frac{dE_x}{dt} = -(\kappa + \gamma_a)E_x - i(\kappa\alpha + \gamma_p)E_x + \kappa(1+i\alpha)(DE_x + inE_y) \quad (1)$$

$$\frac{dE_y}{dt} = -(\kappa - \gamma_a)E_y - i(\kappa\alpha - \gamma_p)E_y + \kappa(1+i\alpha)(DE_y - inE_x) \quad (2)$$

$$\frac{dD}{dt} = -\gamma\left[D\left(1 + |E_x|^2 + |E_y|^2\right) - \mu + in\left(E_yE_x^* - E_xE_y^*\right)\right] \quad (3)$$

$$\frac{dn}{dt} = -\gamma_s n - \gamma\left[n\left(|E_x|^2 + |E_y|^2\right) + iD\left(E_yE_x^* - E_xE_y^*\right)\right] \quad (4)$$

where $E_{x,y}$ are the two linearly polarized slowly varying components of the field and D and n are two carrier variables. In this model x (y) linear polarization has the lowest optical frequency (highest frequency). D accounts for the total population inversion between conduction and valence bands, while n is the difference between the population inversions for the spin-up and spin-down radiation channels. The scaled field is given by $E_{x,y} = \sqrt{G_N/\gamma}\,A_{x,y}$, where $A_{x,y}$ is the cavity field, G_N is the differential gain and γ is the decay rate of D. The scaled total population inversion is given by $D=G_N(N-N_t)/(2\kappa)$, where κ is the field decay rate and N and N_t are the number of carriers in the active region and at transparency, respectively. The same scaling factor is used for n. The rest of VCSEL parameters are as follows: α is the linewidth enhancement factor, μ is the normalized bias current, γ_s is the spin-flip relaxation rate, γ_p is the linear birefringence and γ_a is the linear dichroism. The linear dichroism γ_a is related to the effective dichroism γ_0 by $\gamma_a=(\gamma_0-\gamma_{non})/2$ where γ_{non} is the nonlinear dichroism [13]. The effective dichroism, γ_0, is defined as the difference in the FWHM spectral widths between the two Lorentzian-shaped peaks corresponding to the x and y polarizations, $\Delta\nu_x$ and $\Delta\nu_y$, by $\gamma_0 = \pi(\Delta\nu_x - \Delta\nu_y)$ [13]. The absolute value of γ_0 has a minimum at the current at which PS is observed [13]. γ_{non} is the value of γ_0 at that minimum [13]. Nonlinear dichroism is related to the value of the spin-flip rate by

$$\gamma_s = \kappa(\mu_{PS}-1)\,\gamma/\gamma_{non} \quad (5)$$

where μ_{PS} is the value of the normalized current at the current at which PS occurs [13]. The value of the normalized bias current μ is given in [19]:

$$\mu = \frac{\tau_n}{\tau_e}\frac{\frac{I}{I_{th}} - 1}{1 - \frac{N_t}{N_{th}}} + 1 \quad (6)$$

where τ_e is the differential carrier lifetime at threshold, τ_n is the carrier lifetime at threshold, I is the bias current, I_{th} is the threshold current and N_{th} is the number of carriers at threshold. The substitutition of Eq. (6) evaluated at the PS current I_{PS}, in Eq. (5), and the use of $\gamma=1/\tau_n$ and $\tau_e=e\,N_{th}/I_{th}$ [19] gives

$$\gamma_s = \frac{\kappa}{e\gamma_{non}} \frac{I_{PS} - I_{th}}{N_{th} - N_t} \tag{7}$$

where e is the electron charge. The scaled population inversion at threshold is $D_{th}=G_N(N_{th}-N_t)/(2\kappa)=1-\gamma_a/\kappa$. Using this relation in Eq. (7) we obtain:

$$\gamma_s = \frac{G_N \left(I_{PS} - I_{th} \right)}{2e\gamma_{non} \left(1 - \gamma_a / \kappa \right)} \tag{8}$$

The value of γ_a/κ is much smaller than one. For instance $\gamma_a/\kappa=0.003$ at threshold for the VCSEL of Ref. [19]. Then Eq. (8) is well approximated by:

$$\gamma_s = \frac{G_N \left(I_{PS} - I_{th} \right)}{2e\ \gamma_{non}} \tag{9}$$

This is a simple expression that gives the VCSEL spin-flip rate in terms of quantitities that can be easily measured. This equation gives the temperature dependence of γ_s if G_N, I_{PS}, I_{th} and γ_{non} are measured as a function of the VCSEL substrate temperature, T. Examples of the dependence of G_N, I_{PS}, I_{th} on T can be found in the literature. However, to the best of our knowledge, there are not detailed measurements of γ_{non} as a function of T. These measurements together with the evaluation of the spin-flip rate will be presented in section IV.

3. POLARIZATION CHARACTERISTICS OF THE VCSEL

We have performed measurements on a commercial long-wavelength VCSEL (Raycan [TM]) that emits around 1538 nm. This is the same device that was studied in Refs. [18,19]. A complete set of parameters corresponding to the model of the previous section was measured for T=25°C in [19]. The bias current and temperature are controlled by a laser driver (Thorlabs LDC200) and a temperature controller (Thorlabs TED200), respectively. Our main characterization instrument is a high-resolution optical spectrum analyzer (Aragon Photonics BOSA 210) with 10 MHz of resolution. Our VCSEL is connected to the BOSA by using a FC/APC fiber patch cord. We have minimized the reflections using an index-matching gel in the FC/APC connectors of the VCSEL and the fiber patch cord connected to the BOSA. Also the differential gain is obtained from measuring the oscillation relaxation frequencies as a function of bias current [18]. For this purpose, the VCSEL is connected to an amplified photodetector (Thorlabs PDA8GS) and to an RF-spectrum analyzer (Anritsu MS2719B).

Our VCSEL operates in a single transverse mode with a threshold current of 1.6 mA at T=25°C. The optical spectra of the free-running VCSEL at 4 mA of bias current and T=25°C, can be seen in Fig. 1(b) in Ref. [21]. For this current, the VCSEL emits in the y polarization at λ_y=1538.01 nm and the orthogonal x polarizatio n is shifted 0.23 nm to the long wavelength side λ_x=1538.24 nm (the birefringence of the VCSEL is 28.75 GHz). The polarization resolved light-current characteristics for different values of T are shown in Fig. 1. An increase of I_{th} and a decrease in the slope of the linear part is observed as T increases for the temperature range considered in Fig. 1. Most importantly, we find Type I PS and Type II PS in our device. For low temperatures, T=10 °C, we find a double PS: Type II followed by Type I PS. At intermediate temperature, T=25 °C, we find just Type I PS. For high temperatures, T=40 °C, we find another double PS but opposite to the previous one: Type I followed by Type II PS. Fig. 1 also shows that at the Type II PS the total output power experiences an abrupt drop. This drop is around 1% when T=10°C and around 2 % when T=40°C. This situation is different to that described in [14] in which a similar drop in the total power was observed but for Type I PS to the gain disfavoured mode in a proton implanted VCSEL. The sequence of PS for T=25 and 40 °C is similar to that observed in [7] in which a type I PS appears for relatively low substrate temperatures and for higher temperatures, type I PS followed by type II PS is observed. However Type II followed by Type I PS is not observed in [7] and we do not observe the only type II PS that appears in [7] for still higher substrate temperatures.

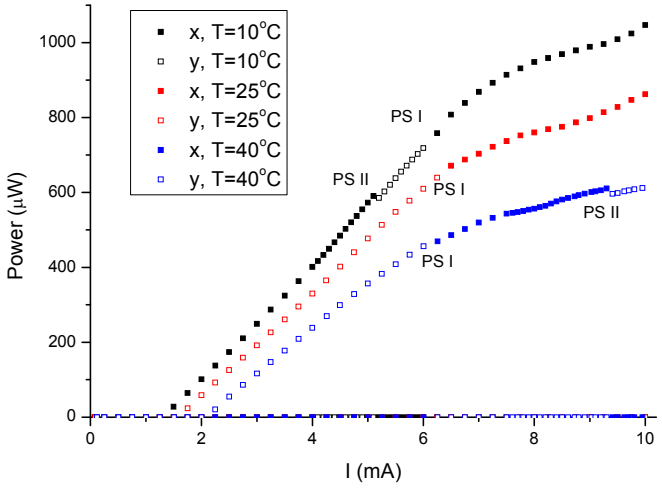

Figure 1. Polarization-resolved light-current characteristics for three different values of the temperature.

We have measured the values of current, I_{PS}, at which both types of PS appear as a function of T. We consider that type I (II) PS happens, when the peak in the optical spectrum corresponding to the low (high) frequency polarization becomes 30 dB above the peak corresponding to the high (low) frequency polarization. The results are shown in Fig. 2. Four different regions appear in this figure. In region I, for temperatures below 7.5ºC, only the *x* polarization is excited and there is not PS at all. In region II, for temperatures between 7.5ºC and 15 ºC, both types of PS appear. For a fixed a value of temperature and increasing the current applied to the VCSEL we find a Type II PS (red color) followed by a Type I PS (black color). The behavior for both types of PS with temperature is different. As temperature is increased, Type II PS appears for lower values of currents, while Type I PS appears for all temperatures around the same value of current, 6mA. In region III, between 15ºC and 35ºC, only Type I PS is found, again for a current near 6 mA. Finally, at higher temperatures, both PS are found again as we can see in the region IV. Nevertheless, in contrast with region II, for a fixed temperature, we find a type I PS followed by a type II PS. As in region II, type II PS appears for lower currents as the temperature is increased, and type I PS remains almost constant with the temperature around 6mA.

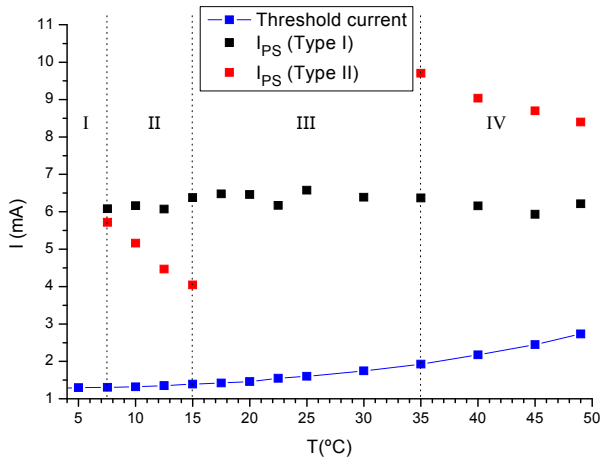

Figure 2. Values of current at which the type I PS (in black color) and type II PS (in red color) appear for different values of temperature. In blue color, the threshold current as a funcion of temperature is represented.

Fig.2 also shows, in blue color, the threshold current for each temperature. The threshold current increases with T for the considered temperature range. The origin of the drop in the total power observed for Type II PS, similarly to [14], is due to the switching to the gain disfavoured (*y*) mode Fig. 3(a) shows the optical spectra for the VCSEL at 40ºC and different values of current to illustrate the Type I-Type II PS sequence. For a current of 5.9 mA, we can see in Fig. 3(a) that the VCSEL emits in the *y* polarization. Fig. 3(b) shows the optical spectrum after Type I PS, for a current of 6.3 mA. Now, the VCSEL emits in the *x* polarization. For higher currents, Fig. 3(c) shows that after Type II PS the VCSEL emits again in the *y* polarization.

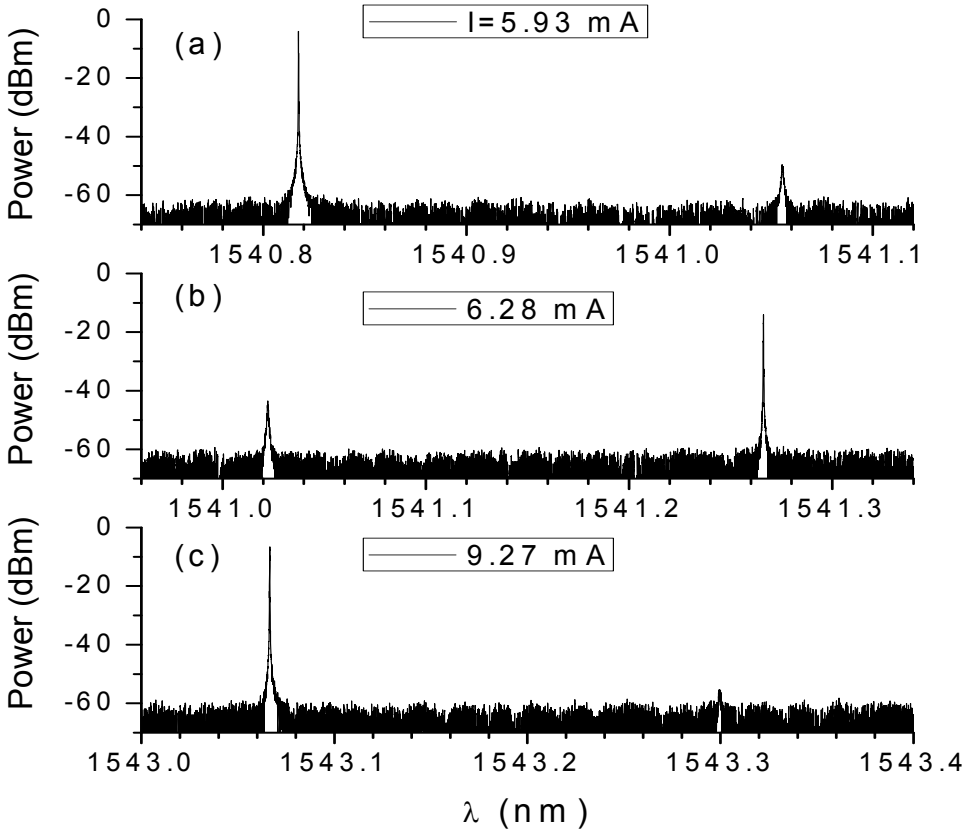

Figure 3. Optical spectra for the free-running VCSEL for a temperature of 40ºC and different values of current (a) 5.93 mA, (b) 6.28 mA, (c) 9.27 mA.

4. DEPENDENCE OF VCSEL POLARIZATION PARAMETERS ON THE TEMPERATURE

In this section we measure the dichroism, birefringence, differential gain and spin-flip rate of the VCSEL as a function of temperature. We first measure the FWHM for both linear polarizations using the BOSA in order to calculate the effective dichroism using $\gamma_0 = \pi(\Delta\nu_x - \Delta\nu_y)$. In Fig. 4 we show $|\gamma_0|$ as a function of the bias current for a value of the temperature in which just Type I PS is obtained (Region III). The absolute value of the effective dichroism, $|\gamma_0|$ presents a minimum at 6.37 mA that coincides with the value of the current at which Type I PS is observed for this temperature. This minimum has also been observed in [13] for 850-nm VCSELs and for the device used in this work [19] at T=25ºC. This minimum is the non-linear dichroism, γ_{non}. We will call $\gamma_{non,1}$ ($\gamma_{non,2}$) the non-linear dichroism that appears near the Type I PS (Type II PS).

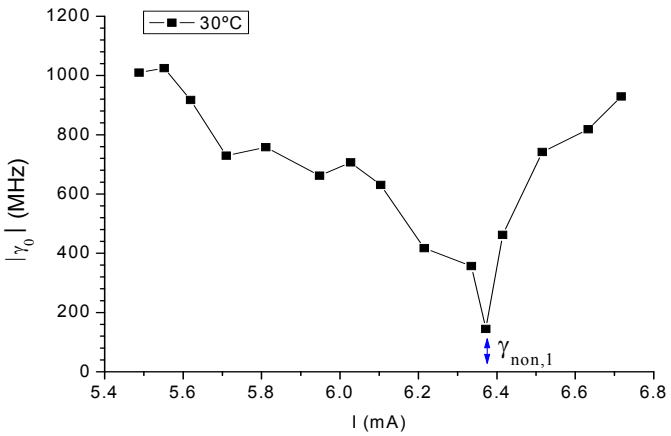

Figure 4. Absolute value of the effective dichroism, $|\gamma_0|$, as a function of the current for T=30ºC. $\gamma_{non,1}$, represents the non-linear dichroism near the type I PS.

Fig. 5 shows $|\gamma_0|$ for (a) 15ºC (region II) and (b) 40ºC (region IV), that is, the regions where double PS is observed. We can see that for both temperatures, $|\gamma_0|$ has two minima: $\gamma_{non,1}$ and an additional minimum, $\gamma_{non,2}$, that appears close to the currents at which Type II PS occurs.

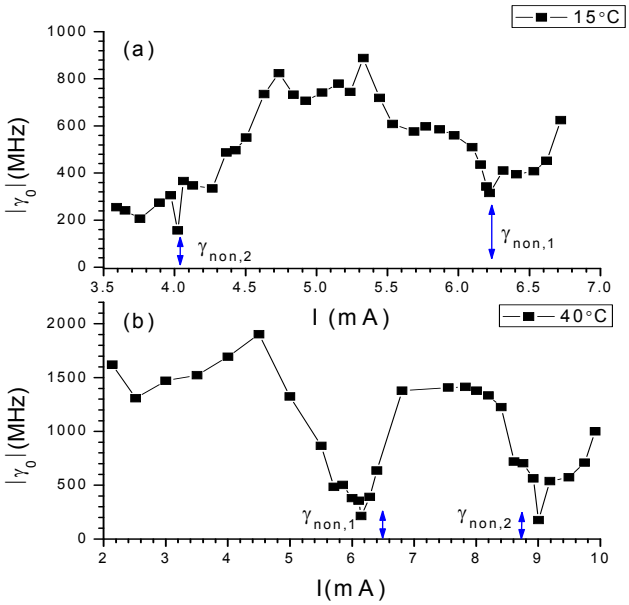

Fig. 5. Absolute value of the effective dichroism, $|\gamma_0|$, as a function of the current for (a) 15ºC, and (b) 40ºC, respectively. The values of nonlinear dichroism near the type I and type II PS, $\gamma_{non,1}$ and $\gamma_{non,2}$ respectively, are also indicated

We have measured the non-linear dichroism for the whole range of temperatures and for both types of PS. Fig. 6 shows with black squares the non-linear dichroism obtained near (a) type I PS and (b) type II PS, respectively. Fig. 6 (a) shows two different tendencies for $\gamma_{non,1}$, below and above 40 ºC. Below 40ºC, $\gamma_{non,1}$ decreases as the temperature is increased, but a small increase for the value of $\gamma_{non,1}$ appears at 40ºC. From this temperature onwards, $\gamma_{non,1}$ decreases again as the temperature is increased. Fig. 6(b) shows the non-linear dichroism, $\gamma_{non,2}$, obtained near type II PS. The highest values for $\gamma_{non,2}$, 0.32 ns^{-1} and 0.33 ns^{-1} are found for 10ºC and 12.5 ºC, respectively. For the rest of temperatures, the measured value for $\gamma_{non,2}$ is around 0.15 ns^{-1} except for 45ºC where the value obtained is slightly higher, 0.24 ns^{-1}.

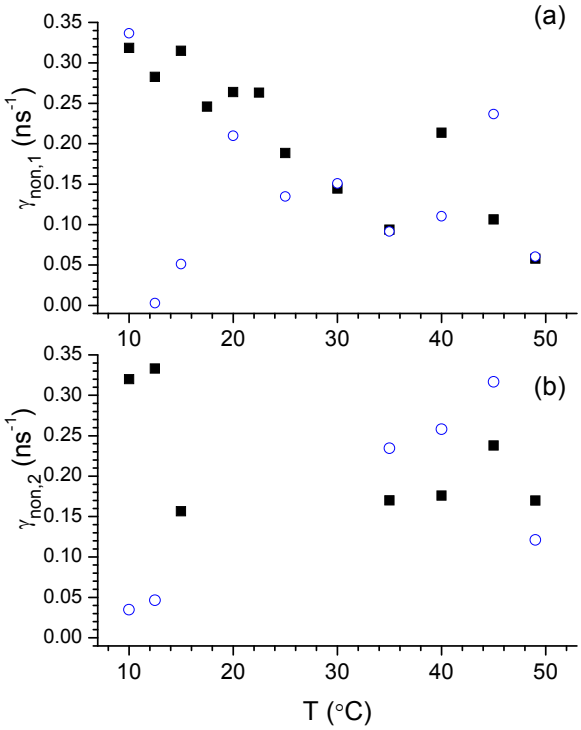

Fig. 6. Non-linear dichroism as a function of the temperature for (a) type I PS, $\gamma_{non,1,}$ and for (b) type II PS, $\gamma_{non,2}$. Results are obtained from the minimum of $|\gamma_0|$ (black squares) and from the nonlinear birefringence, $\Delta\nu_0$ (blue circles).

The linear birefringence parameter, γ_p, can be obtained from the frequency splitting between the y and the x polarizations, the so-called effective birefringence. Fig. 7a and Fig. 7b show the values of the effective birefringence as a function of the current for 10ºC and 40ºC, respectively. For 10ºC, the birefringence oscillates around 29.25 GHz and the period of the oscillations is around 0.8mA. These values are similar to those found in [19] for a temperature of 25ºC and the same device. However, when the temperature is 40ºC and until 8 mA, the mean value of the birefringence decreases as the current increases from 30.6 GHz to 29.4 GHz approximately. The oxide-confined devices exhibit a strong decrease of the frequency splitting when the current is increased [15]. It has also been observed in proton-implanted VCSELs for currents smaller than the PS current [16]. From 8mA onwards, the birefringence oscillates around a constant value 29.75 GHz. For the whole range of current, the period of the oscillations is around 0.64 mA. A possible reason for these oscillations is the existence of weak optical feedback in the experiment [19], [22].

Discontinuities in the effective birefringence have been observed for the whole range of temperatures at currents at which PSs are observed [13], [19]. The birefringence jump is also called nonlinear birefringence, $\Delta\nu_0$. Fig. 7a and Fig. 7b show some of these discontinuities. Fig. 8 shows the nonlinear birefringence for the whole range of temperatures. In black (red) color is represented the nonlinear birefringence obtained for the currents at which type I PS (type II PS) happens. For 15ºC, $\Delta\nu_0$ near the current of type II PS was not observed, probably because it happens in a very small range of currents difficult to measure. Nonlinear dichroism is related to the nonlinear birefringence by $\gamma_{non}=\pi\Delta\nu_0/\alpha$ [13]. We have used this expression to evaluate $\gamma_{non,1}$ and $\gamma_{non,2}$ from the data included in Fig. 8. The results are shown using blue circles in Fig. 6. These values are rather similar to those obtained by using the nonlinear dichroism; there are only significant discrepancies for some points at T=10, 12.5 and 15 ^{o}C but, apart from these points, the qualitative tendencies of both sets of results are similar.

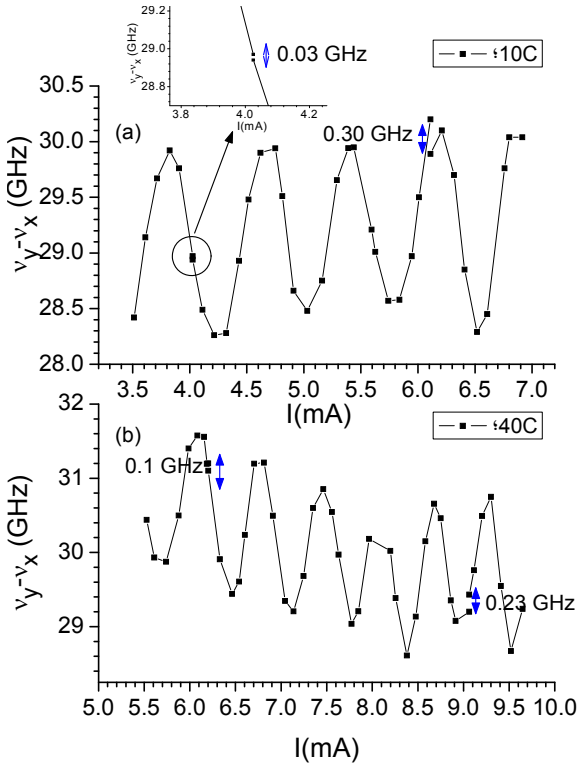

Fig.7. Effective birefringence as a function of the current for (a) 10ºC and (b) 40ºC. Values of the birefringence jumps are also indicated.

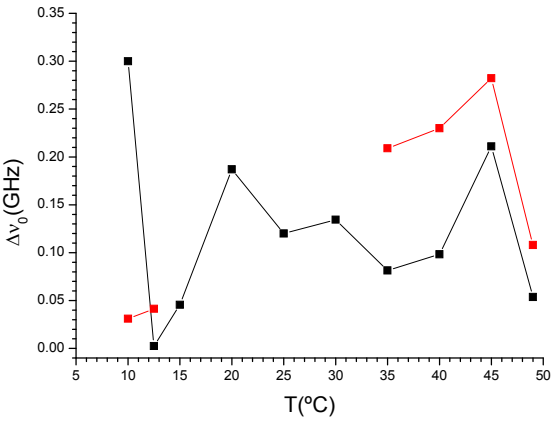

Fig.8. (a) Nonlinear birefringence as a function of the temperature. In black (red) color is represented the value of the nonlinear birefringence obtained for the currents at which type I PS (type II PS) happens.

The differential gain as a function of T can be obtained from intensity noise spectra measurements. Amplitude noise power spectra for several values of the bias current and 25ºC can be found in [18] for this device. The measured noise spectra for every temperature and for several currents below 2 times threshold, are smoothed with an adjacent-averaging smoothing to determine the frequency of the resonance peak, that approximately corresponds to the relaxation oscillation frequency, f_R. The validity of this approximation is discussed in [18]. This frequency is related to the angular relaxation oscillation frequency Ω_R by $\Omega_R=2\pi f_R$, and the differential gain for each value of T is obtained by a linear fitting of the

following expression $\Omega_R^2=G_N(I-I_{th})/e$ [23]. Fig. 9 represents the differential gain for the whole range of temperatures. Two different behaviors are identified for the differential gain. For temperatures below 25ºC, the differential gain increases linearly with the temperature. However, the behavior changes for higher temperatures, where the differential gain decreases rapidly with the increase of temperature. Previous works have studied the temperature dependence of the differential gain theoretically [2], [24] and experimentally, for long and short-wavelength VCSELs [25, 26], respectively. Our temperature dependence of G_N is similar to that found theoretically [24] and experimentally [25] for long-wavelength VCSELs. The variations in differential gain depend on the room-temperature offset between the gain peak wavelength and the wavelength of the lasing mode [24]. For large offsets, the differential gain increases with temperature until the cavity mode passes the gain peak. Then, as the temperature increases, the differential gain decreases [24]. In our device, the maximum value of the differential gain is reached for a room temperature of 25ºC.

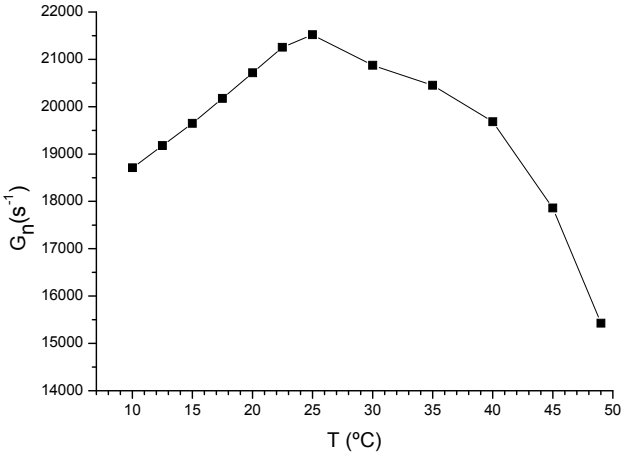

Fig.9. Differential gain as a function of the temperature.

The value of the spin-flip rate can be obtained by using Eq. (9). The temperature dependence of γ_s can now be found as we have measured this dependence for G_N, I_{PS}, I_{th} and γ_{non}. For each type of PS we have obtained a set of values of I_{PS} and γ_{non}, as it can be seen from Fig. 2 and Fig. 6. Eq. (9) gives then two independent estimations for γ_s. Fig. 10 shows the dependence of γ_s with T obtained with Type I and Type II PS data. In this figure we have used the values of γ_{non} obtained from the nonlinear dichroism.

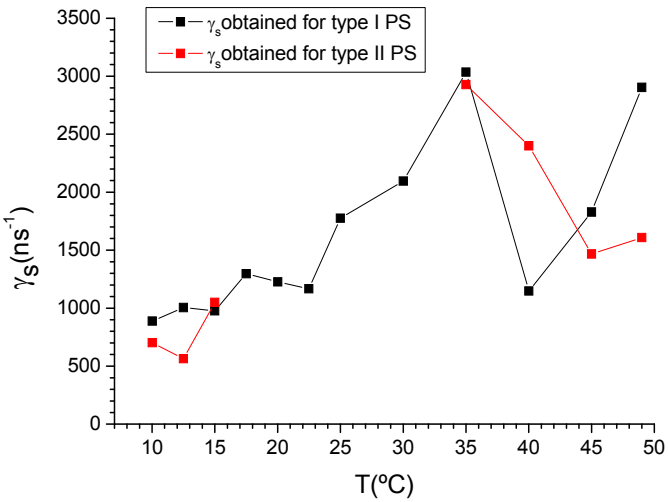

Fig.10. Spin-flip rate as a function of the temperature. Black (Red) colour represents the values obtained for the spin-flip rate at the currents at which type I (type II) PS appear.

The spin-flip rate obtained for Type I PS, in general, tends to increase as the temperature is increased up to 35ºC. At this temperature γ_s, decreases from 3000 ns^{-1} to 1100 ns^{-1} at T=40ºC. For higher temperatures, γ_s increases again. The qualitative trend of γ_s is mainly given by that of $\gamma_{non,1}$. γ_s increases with T because $\gamma_{non,1}$ decreases with T with the exception of the local minimum that appears close to T=40 ºC, at which temperature $\gamma_{non,1}$ has a local maximum. The spin-flip rate obtained from Type II PS data is in general consistent with that obtained from Type I data. The observed discrepancies can be mainly attributted to the high value of the relative error of γ_s (around 25 %) [19].

5. SUMMARY

Different mechanisms have been proposed to explain type I polarization switching. It could be attributed to thermal effects [5], photon energy-dependent loss [7], thermal lensing [11], modal gain changes due to the change of carrier distribution [8] or in the framework of the spin-flip model (SFM) in terms of phase instabilities driven by the spin-flip mechanism which is represented by γ_s [6]. In our case, the origin of the type I PS is not clear [19]. It looks that it is not due to thermal effects as it remains constant with the temperature [15]. Similarly, the reasons for the Type II PS are not clear. Further analysis has to be done to clarify the origin of both types of PS.

In this work Type I PS (from the high- frequency to the low frequency polarization) and type II PS (from the low-frequency to the high-frequency polarization) have been found in a long-wavelength VCSEL for different values of VCSEL temperatures. For low temperatures, Type II PS followed by Type I PS as the current increases has been found. Increasing the temperature we find only a type I PS. Further increase of the temperature leads to Type I PS followed by Type II PS. To the best of our knowledge this is the first observation of a double PS consisting on a type II PS followed by a Type I PS. Type II PS appears for lower currents as the temperature applied to the VCSEL increases while the current at which Type I PS appears does not change with temperature. Type II PSs are characterized by a drop in the total power that corresponds to a switching to the gain disfavoured mode.

We have measured PS current, effective dichroism and birefringence, differential gain and threshold current as a function of the temperature. The modulus of the effective dichroism, the nonlinear dichroism, can have several minima at the temperatures at which PSs are observed. These minima have been related to the nonlinear birefringence. We have also derived a simple expression for the spin-flip rate combining the PS current, nonlinear dichroism, differential gain and threshold current. Using this expression we have obtained the values of the spin-flip rate and its temperature dependence, which is mainly given by the dependence of the inverse of the nonlinear dichroism with the temperature.

ACKNOWLEDGMENTS

This work has been funded by the Ministerio de Economía y Competitividad, Spain under project TEC2012-38864-C03-03 and cofinanced by FEDER funds. A. Quirce acknowledges FWO for her Post Doc fellowship and H. Thienpont and K. Panajotov are grateful to the Methusalem foundation for financial support.

REFERENCES

1. R.Michalzik, VCSELs: Fundamentals, Technology, and Applications of Vertical-Cavity Surface-Emitting Lasers. Berlin, Germany, Springer-Verlag, 2012.
2. S. F. Yu, Analysis and design of Vertical-Cavity Surface-Emitting Lasers, Semiconductors, New Jersey: Wiley-Interscience, 2003.
3. F. Koyama, "Recent advances of VCSEL photonics," J. Lightw. Technol., vol. 24, no. 12, pp. 4502-4513, Dec. 2006.
4. V. Iakovlev, A. Sirbu, Z. Mickovic, D. Ellafi, G. Suruceanu, A. Mereuta, A. Caliman, and E. Kapon, "Progresses and challenges in industrial fabrication of wafer-fused VCSELs emitting in the 1310 nm band for high speed wavelength división multiplexing applications,"Proc. SPIE **8639**, 863904, 2013.
5. K.D. Choquette, R.P. Schneider, K. L. Lear, and R. E. Leibenguth, "Gain-dependent polarization properties of vertical-cavity lasers," IEEE J. Sel. Top. Quantum Electron. vol. 1, no. 2, pp. 661-666, Jun. 1995.
6. M. San Miguel, Q. Feng and J. V. Moloney, "Light-Polarization Dynamics in Surface-Emitting Semiconductor-Lasers,"Physical Review A, vol. 52, no. 2, pp. 1728-1739, Aug. 1995.

7. B. Ryvkin, K. Panajotov, A. Georgievski, J. Danckaert, M. Peeters, G. Verschaffelt, H. Thienpont, and I. Veretennicoff, “Effect of photon-energy dependent loss and gain mechanisms on polarization switching in vertical cavity surface-emitting lasers,” J. Opt. Soc. Amer. B, vol.16, no. 11, pp. 2106-2113, Nov. 1999.
8. A. Valle, L. Pesquera, and K. A. Shore, “Polarization behavior of birefringent multitransverse mode vertical-cavity surface-emitting lasers,” IEEE Photon. Technol. Lett., vol. 9, no. 5, pp. 557-559, May 1997.
9. D. Vakhshoori, J. D. Wynn, G. J. Zydzik, M. Asom, K. Kojima, R. E. Leibenguth, and R. A. Morgan, “Top-surface emitting lasers with 1.9 V threshold voltage and the effect of spatial hole burning on their transverse mode operation and characteristics,” Appl. Phys. Lett., vol. 62, no. 13, pp. 1448-1450, 1993.
10. J. Mulet and S. Balle, "Spatio-Temporal Modeling of the Optical Properties of VCSELs in the Presence of Polarization Effects," IEEE J. Quant. Electron., vol. 38, no. 3, pp. 291-305, Mar. 2002.
11. K. Panajotov, B. Ryvkin, J. Dackaert, M. Peeters, H: Thienpont, I. Veretennicoff “Polarization switching in VCSELs due to thermal lensing,” IEEE Photon. Technol. Lett. vol.10, no. 1, pp.6-8, Jan., 1998.
12. M. Sondermann, T. Ackemann, S. Balle, J. Mulet, and K. Panajotov, “Experimental and theoretical investigations on elliptically polarized dynamical transition states in the polarization switching of vertical-cavity surface-emitting lasers,” Opt. Commun. vol. 235, no. 4-6, pp. 421-434, May, 2004.
13. M. P. van Exter, M. B. Willemsen, and J. P. Woerdman, “Polarization fluctuations in vertical-cavity semiconductor lasers,” Phys. Rev. A, vol. 58, no. 5, pp. 4191-4205, Nov. 1998.
14. M. Sondermann, M. Weinkath, and T. Ackemann, “Polarization switching to the gain disfavored mode in vertical-cavity surface-emitting lasers,” IEEE. J. Quantum Electron., vol. 40, no. 2, pp. 97-104, Feb. 2004.
15. G. Verschaffelt, K. Panajotov, J. Albert, B. Nagler, M. Peeters, J. Danckaert, I. Veretennicoff, and H. Thienpont, “Polarization switching in vertical-cavity surface-emitting laser”. Optoelectron. Rev. vol. 9, no.3, pp. 257-268, 2001.
16. T. Ackeman and M Sondermann, “Characteristics of polarization switching from the low to the high frequency mode in vertical-cavity surface-emitting lasers”. Appl. Phys. Lett. vol. 78, pp. 3574-3576, Apr. 2001.
17. T. Deng, Z. M. Wu, Y. Y. Xie, J. G. Wu, X. Tang, L. Fan, K. Panajotov, and G.Q. Xia, “Impact of optical feedback on current-induced polarization behavior of 1550-nm vertical-cavity surface-emitting lasers,” Appl. Opt. vol. 52, pp. 3833-3837, 2013.
18. P. Pérez, A. Valle, I. Noriega, and L. Pesquera “Measurement of the Intrinsic Parameters of Single-Mode VCSELs,” J. of Lightwave Technology, vol. 32, no. 8, pp. 1601-1607, Apr. 2014.
19. P. Pérez, A. Valle, and L. Pesquera, “Polarization-resolved characterization of long-wavelength vertical-cavity surface-emitting laser parameters,” J. Opt. Soc. Am. B., vol. 31, no. 11, pp. 2574-2580, Nov. 2014.
20. J. Martín-Regalado, F. Prati, M. San Miguel, and N. B. Abraham, “Polarization properties of vertical-cavity surface-emitting lasers,” IEEE J. Quantum Electron. vol. 33, no. 5, pp. 765-783, May 1997.
21. A. Quirce, P. Pérez, H. Lin, A. Valle, L. Pesquera, K. Panajotov, and H. Thienpont “Polarization Switching Regions of Optically Injected Long-Wavelength VCSELs,” IEEE J. Quantum Electron., vol. 50, no. 11, pp. 921-928, Nov.2014.
22. M. A. Arteaga, H. J. Unold, J. M. Ostermann, R. Michalzik, H. Thienpont, K. Panajotov, “Investigation of polarization properties of VCSELs subject to optical feedback from an extremly short external cavity-part I: theoretical analysis,” IEEE J. Quant. Electron., vol. 42, no. 2, pp. 89-101, 2006.
23. G.P. Agrawal, N. K. Dutta, “Long-wavelength semiconductor lasers”, Van Nostrand Reinhold Co. 1986.
24. E. S. Björlin, J. Geske, M. Mehta, J. Piprek, J. E. Bowers, “Temperature dependence of the relaxation resonance frequency of long-wavelength vertical-cavity lasers”, IEEE Photonics Technology Letters., vol.17, no. 5, pp. 944-946, May 2005.
25. N. A. Khan, K. Schires, A. Hurtado, I. D. Henning, M. J. Adams, “Measurement of temperature-dependent relaxation oscillation frequency and linewidth enhancement factor of a 1550 nm VCSEL”, IEEE J. Quantum Electron., vol. 49, no. 11, pp. 990-996, Nov. 2013.
26. R. Safaisini, J. R. Joseph, D. Louderback, X. Jin, A. N. Al-Omari, K. L. Lear, “Temperature dependence of 980-nm oxide-confined VCSEL dynamics”, IEEE Photonics Technology Letters, vol. 20, no. 14, pp. 1273-1275, Jul. 2008.